Journal of Alloys and Compounds 509 (2011) 2227–2231

Contents lists available at ScienceDirect

Journal of Alloys and Compounds

journal homepage: www.elsevier.com/locate/jallcom

High quality GaN epilayers grown on Si (1 1 1) with thin nonlinearly composition-graded $Al_xGa_{1-x}N$ interlayers via metal-organic chemical vapor deposition

R.F. Xiang[a], Y.-Y. Fang[a,b,*], J.N. Dai[a,b], L. Zhang[a], C.Y. Su[a], Z.H. Wu[a,b], C.H. Yu[a], H. Xiong[a,b], C.Q. Chen[a,b], Y. Hao[a,c]

[a] Wuhan National Laboratory for Optoelectronics, School of Optoelectronic Science and Engineering, Huazhong University of Science and Technology, Wuhan 430074, China
[b] State Key Laboratory of Functional Materials for Informatics, Shanghai Institute of Microsystem and Information Technology, Chinese Academy of Sciences, 865 Changning Road, Shanghai 200050, China
[c] Key Laboratory for Wide Band-Gap Semiconductor Materials and Devices of the Ministry of Education, School of Microelectronics, Xidian University, Xi'an 710071, China

ARTICLE INFO

Article history:
Received 22 July 2010
Received in revised form 28 October 2010
Accepted 29 October 2010
Available online 10 November 2010

Keywords:
Gallium nitride (GaN)
Si (1 1 1) substrates
Metal-organic chemical vapor deposition (MOCVD)
$Al_xGa_{1-x}N$ interlayer

ABSTRACT

The growth of GaN epilayers on AlN/Si (1 1 1) templates with thin nonlinearly composition-graded $Al_xGa_{1-x}N$ interlayers via metal-organic chemical vapor deposition (MOCVD) is reported in this work. The composition-graded $Al_xGa_{1-x}N$ interlayer was achieved by simply changing the growth condition of AlN to that of GaN layers during a fixed time. The surface morphology, crystalline quality and stress of GaN films have been investigated with different $Al_xGa_{1-x}N$ interlayer thickness, 280 nm, 460 nm, 575 nm, and 750 nm. It was found that the properties of GaN films are highly dependent on the $Al_xGa_{1-x}N$ interlayer thickness. High quality crack-free GaN films up to 1.2 μm can be achieved with 460 nm thick $Al_xGa_{1-x}N$ layer.

1. Introduction

Heteroepitaxial growth of GaN on silicon has been attracting increasing attention due to numerous advantages of this substrate, including low cost, large scale availability, good thermal conductivity and potential applications in integrated optoelectronic devices [1–4]. However, the large lattice mismatch between GaN and Si results in high dislocation density, which is of the order of $\sim 10^{10}$ cm^{-2}, and their great difference in thermal expansion coefficient (~56%) always leads to large tensile stress, which results in cracking of the GaN layer during cooling-down process [1–21]. These finally degrade the performance of GaN-based devices. Therefore, the key issue to fabricate GaN-based devices using Si substrates is to grow high quality, low dislocation density and crack-free GaN epilayers.

The design of buffer layer structure for strain engineering and dislocation reduction has been considered to be crucial for the growth of high quality GaN on Si substrates. Different techniques have been used by some groups to obtain thick crack-free and high quality GaN layer successfully. Low-temperature (LT) AlN interlayers for GaN grown on Si were first applied by Krost et al. [1,2], and some improvements were made by other groups [5,6]. Some techniques originally used for the growth of III-nitrides on sapphire or SiC substrates, such as AlGaN interlayers [7], AlN/GaN- or AlGaN/GaN-based superlattices [8,9], were applied for GaN epitaxy on Si substrates. Besides these routine techniques, several novel approaches showing excellent effects in strain control and dislocations reduction, for example, step-graded $Al_xGa_{1-x}N$ interlayers [10–12,16], composition-graded $Al_xGa_{1-x}N$ interlayer [13–17], AlInN interlayers [18], InN interlayers [19] and etc., have also been developed. For all these techniques, it has been noticed that the growth parameters of the buffer layer, such as growth temperature, thickness, and V/III ratio, affect the quality of GaN greatly, indicating the precise optimization of the growth parameters and detailed study of the stress relaxation mechanisms are essential. Furthermore, it has been found that the graded-$Al_xGa_{1-x}N$-layer technique, including step-graded and composition-graded $Al_xGa_{1-x}N$-layer, exhibits superiority for the growth of GaN layers on large-size Si substrates [11,17]. As far as the composition-graded $Al_xGa_{1-x}N$-layer technique is concerned, the gradual change of lattice constants and thermal expansion

* Corresponding author at: Wuhan National Laboratory for Optoelectronics, School of Optoelectronic Science and Engineering, Huazhong University of Science and Technology, 1037 Luoyu Road, Wuhan 430074, Hubei Province, China.
Tel.: +86 27 87793024; fax: +86 27 87793035.
E-mail address: yanyanfang.hust@gmail.com (Y.-Y. Fang).

0925-8388/$ – see front matter © 2010 Elsevier B.V. All rights reserved.
doi:10.1016/j.jallcom.2010.10.189

coefficient from AlN to GaN, facilitating the introduction of compressive strain and accommodation of the large thermal mismatch, can effectively compensate the tensile stress and reduce threading dislocations in GaN layer. Therefore, linearly graded layers are usually designed for this purpose. However, the growth condition has to be precisely controlled in order to achieve the linearly graded composition versus thickness. To circumvent the relatively complicate growth process, a more straightforward method of growing graded-$Al_xGa_{1-x}N$ interlayer, which is simply changing the growth condition from AlN recipe to GaN recipe during a fixed time was proposed. Although there are some reports on this method [13,14], the detailed study of the effect of composition-graded $Al_xGa_{1-x}N$ interlayer thickness has not been fully explored.

In this work, we grew a series of GaN epilayers on Si (1 1 1) by using high temperature (HT) AlN and composition-graded interlayer buffering techniques, as Fig. 1 shows. By varying the thickness of continuously composition-graded $Al_xGa_{1-x}N$ interlayer, the optimized thickness was obtained and a systematic study of the stress relaxation mechanisms was conducted. The results show that at the optimum $Al_xGa_{1-x}N$ interlayer thickness of about 460 nm, high quality and crack-free GaN epilayers up to 1.2 μm can be routinely grown.

2. Experimental details

GaN epitaxial layers on Si (1 1 1) substrates were grown in a Thomas Swan CCS IC6 × 2 metal-organic chemical vapor deposition (MOCVD) reactor. Hydrogen was used as carrier gas, and trimethylaluminium (TMAl), trimethylgallium (TMGa), and ammonia were used as the precursors for Ga, Al and N, respectively. The Si (1 1 1) substrate was first passivated by TMAl for 15 s at 1100 °C to avoid the formation of amorphous Si_xN_y. Then, a 300-nm thick HT-AlN buffer layer was deposited, followed by a continuously composition-graded $Al_xGa_{1-x}N$ interlayer. After that, a 1.2 μm-thick GaN epilayer was grown at 1050 °C. Here, the composition of $Al_xGa_{1-x}N$ interlayer was changed from AlN to GaN continuously by simply changing the growth condition from AlN recipe to GaN recipe, which was varying the source flux and growth temperature simultaneously. In order to investigate the effect of $Al_xGa_{1-x}N$ interlayer on the subsequently grown GaN, the growth time of $Al_xGa_{1-x}N$ interlayer was set for 800 s, 1500 s, 1900 s and 2300 s. The samples are denoted as A, B, C and D, respectively. The thickness of $Al_xGa_{1-x}N$ interlayer was estimated by *in-situ* interferometer to be about 280 nm, 460 nm, 575 nm, and 750 nm for samples A–D, respectively.

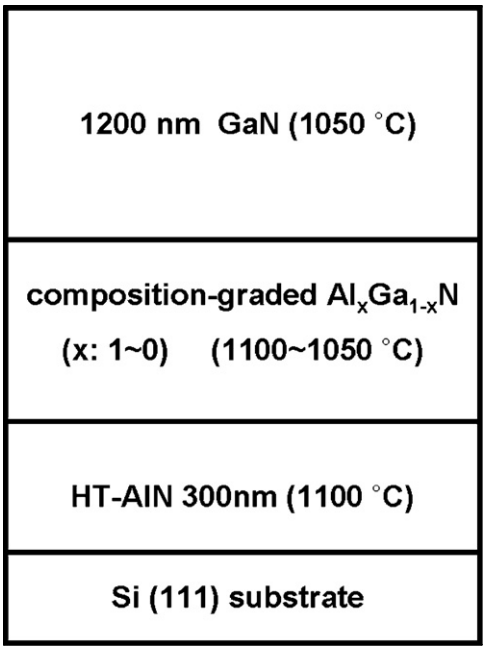

Fig. 1. Schematic structure of the samples grown. Thickness of $Al_xGa_{1-x}N$ intermediate layer was varied by the change of the growth time.

The crack density and distribution of the as-grown samples were examined by Olympus-BX51 differential interference contrast (DIC) microscopy. The surface morphology was studied by atomic force microscope (AFM) in contact mode (Veeco NanoScope MultiMode). And the crystallinity of the samples was investigated using high-resolution X-ray diffraction (HR-XRD, PANalytical X'pert Pro MRD) with Cu Kα1 (λ = 1.5405974 Å) as source for X-ray rocking curves (XRC) measurements. The tensile stress of the GaN samples was determined by Raman frequency shift from Raman

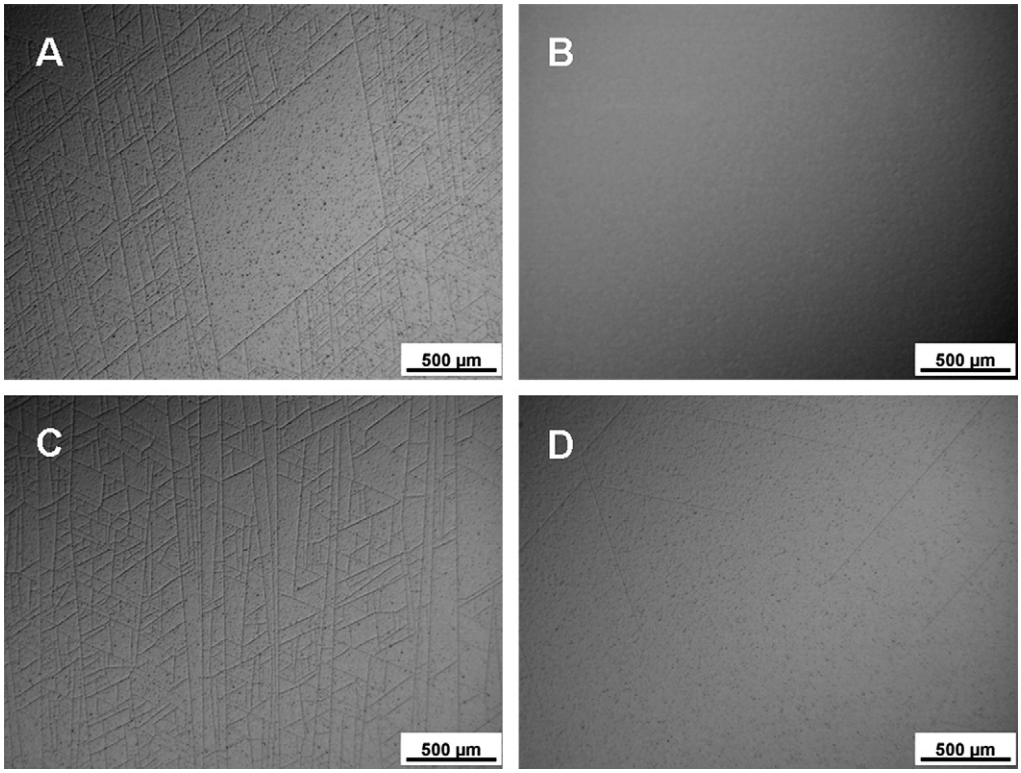

Fig. 2. Optical micrographs of samples A–D.

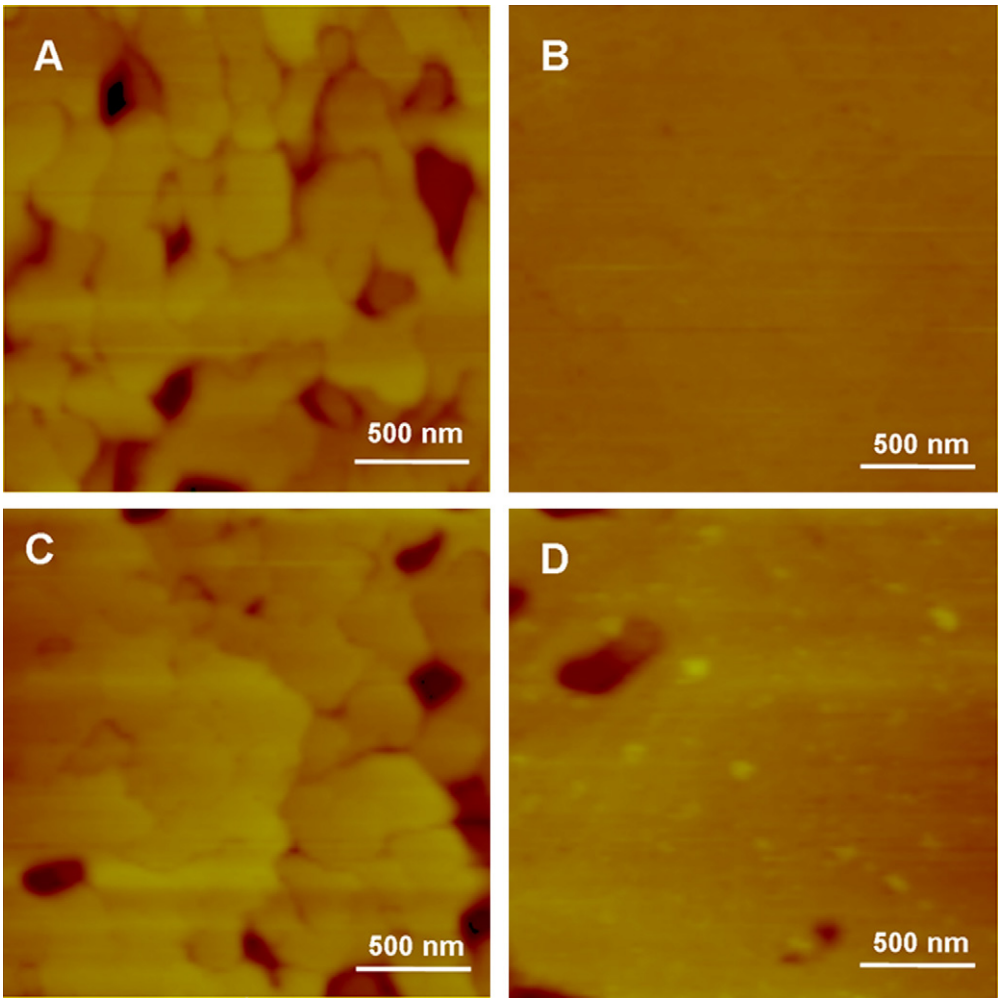

Fig. 3. AFM images of GaN surfaces with scan area of 2 μm × 2 μm. The RMS roughness is 3.458 nm, 0.558 nm, 3.644 nm, 2.049 for A–D, respectively.

spectra (HR800UV Raman spectrometer using 514 nm laser.). Lattice constants and strain states were obtained from reciprocal space maps (RSMs) by HR-XRD.

3. Results and discussion

The optical micrographs in Fig. 2 show the crack density and distribution of samples A–D. Sample A and C have relatively higher crack density than sample D, while sample B is crack-free. Most cracks propagate during cooling process due to the large tensile stress resulting from difference of thermal expansion coefficient between GaN and Si. Cracks usually originate from defects, such as pits, pin-holes, and V-shaped defects, thus the crack density always increases with the increasing defect density [20]. Therefore, GaN samples with high density of cracks often bear poor crystalline quality and high defect density. Accordingly, sample B has the best crystallinity and lowest defect density. This can be further affirmed by the full-width-half-maximum (FWHM) of XRCs, which will be discussed in detail later.

In addition, we compare the surface morphology of samples A–D by the AFM study as Fig. 3 shows. Sample A and C have quite rough surface (root-mean-square (RMS) roughness is 3.458 nm, 3.664 nm, respectively) with not fully coalesced islands, sample D has a large flat area and some occasionally uncoalesced islands, while sample B has very flat surface (RMS roughness is 0.558 nm) without obvious uncoalesced islands. Since the threading dislocations, the main defects of GaN layers, originate from the twist and tilt of slightly misaligned mosaic grains, thus the defect density usually decreases with the increasing grain size. Consequently, the surface features are closely related to the defect density of the material. The smooth surface in sample B suggests that the growth mode in sample B is more like two dimensional epitaxy, leading larger island size and lower dislocation density. While in sample A and C, the growth mode is more like three dimensional island growth, leading to smaller island and higher dislocation density. In all, sample B has the lowest dislocation density, which is consistent with what has been observed from the optical micrograph. We also notice that with the further increase of $Al_xGa_{1-x}N$ interlayer, the defect density of GaN epilayers ascends first, and then descends.

Fig. 4 compares the room temperature Raman spectrum of samples A–D, obtained with 514 nm excitation. As the inset shows, the Raman shifts of the GaN E_2 (TO) phonon peak of sample A–D are 563.96, 566.13, 565.12, and 565.58 cm^{-1}, respectively. The residual stress for each sample was calculated using the E_2 (TO) phonon peaks 567.50 cm^{-1} for a 400-μm-thick, freestanding and strain-free GaN and the relation $\Delta\omega = K\sigma_{xx}$ cm^{-1} GPa^{-1}. Here $\Delta\omega$ is the phonon peak shift, σ is the biaxial stress, and $K = 4.3$ is the pressure coefficient [21]. The calculated tensile stresses in these GaN films are 0.824 GPa, 0.319 GPa, 0.553 GPa, and 0.447 GPa, respectively (Fig. 5). The results demonstrate that the $Al_xGa_{1-x}N$ interlayer can compensate the tensile stress in GaN film. Interestingly, unlike the behavior reported in other papers [13–15], which states that the thicker the $Al_xGa_{1-x}N$ interlayer is, the less stress exists in GaN film and usually a $Al_xGa_{1-x}N$ interlayer up to 800–1000 nm thick is needed to grown crack-free thick GaN, we found in our case a min-

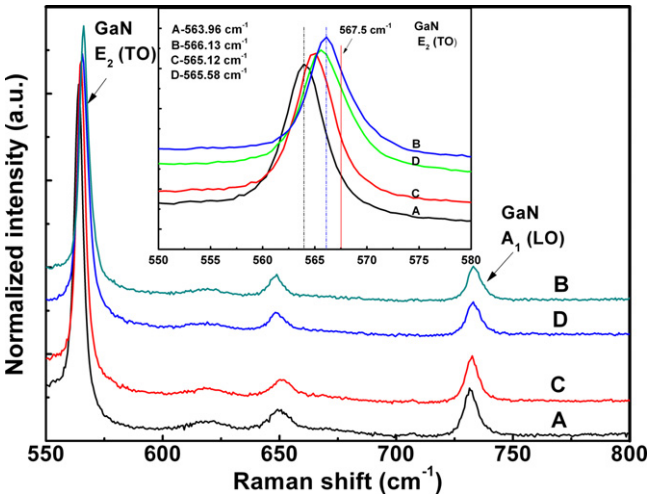

Fig. 4. Raman spectra of four GaN samples (from top to bottom, are samples B, D, C, A, respectively), and the inset shows enlarged picture of GaN E_2 (TO) mode.

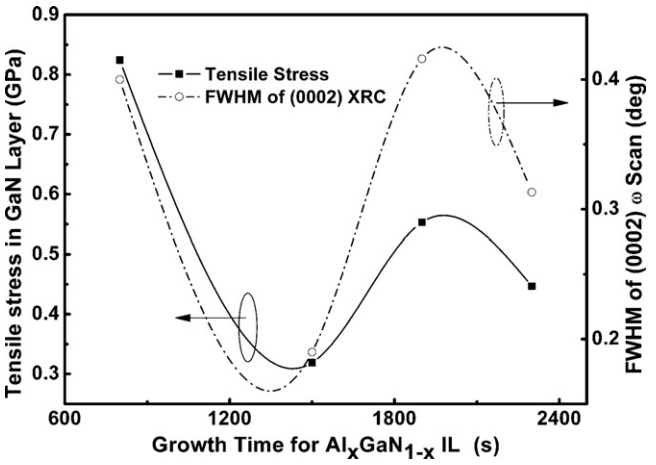

Fig. 5. Tensile stress (Raman results) and corresponding (0 0 0 2) FWHM of GaN films versus the growth time of the $Al_xGa_{1-x}N$ interlayer.

imum stress in GaN film appeared when the $Al_xGa_{1-x}N$ interlayer is only 460 nm thick.

The crystallinity and strain states in these four GaN samples were further investigated by recording the XRCs and RSMs for the symmetric (0 0 0 2) and asymmetric ($10\bar{1}5$) Bragg reflections. As we expect, the (0 0 0 2) FWHM of sample B is the smallest (sample A is 0.41°, B is 0.193°, C is 0.416°, and D is 0.313°, respectively), which agrees well with the results of optical microscope and AFM. Fig. 5 shows the behavior of tensile stress (Raman results) and corresponding (0 0 0 2) FWHM versus the growth time of the $Al_xGa_{1-x}N$ interlayer. It is obvious that the less the tensile stress, the better the crystalline quality. Moreover, the stress of the GaN epilayer does not monotonously change with the increasing thickness of $Al_xGa_{1-x}N$ interlayer.

Fig. 6 exhibits the (0 0 0 2) RSMs and ($10\bar{1}5$) RSMs of sample B. From symmetric (0 0 0 2) RSM, the good vertical alignment of AlN, $Al_xGa_{1-x}N$ and GaN peaks indicates a coherent heterostructure. The asymmetric ($10\bar{1}5$) RSMs exhibit considerable offset of the respective AlN, $Al_xGa_{1-x}N$ and GaN peaks with respect to the relaxation line, illustrating the significant tensile strain in AlN and GaN layers, and the transition of compressive strain to tensile strain in $Al_xGa_{1-x}N$ interlayer. Moreover, the strain can be calculated from a, c lattice constants. The lattice constants of GaN and AlN are $c_{meas}^{GaN} = 5.1828$ Å, $a_{meas}^{GaN} = 3.1933$ Å, $c_{meas}^{AlN} = 4.9713$ Å, and $a_{meas}^{AlN} = 3.1292$ Å, respectively. Related to the bulk values, ($c_{0,GaN} = 5.1850$ Å, $a_{0,GaN} = 3.1892$ Å, $c_{0,AlN} = 4.9810$ Å, and $a_{0,AlN} = 3.1112$ Å) [22], the strains of GaN and AlN can be acquired from the definition,

$$\varepsilon_a = \left[\frac{(a_{meas} - a_0)}{a_0}\right] \times 100\%, \quad \varepsilon_c = \left[\frac{(c_{meas} - c_0)}{c_0}\right] \times 100\%. \qquad (1)$$

Thus, we obtain $\varepsilon_{a,GaN} = 0.129\%$, $\varepsilon_{c,GaN} = -0.042\%$, $\varepsilon_{a,AlN} = 0.578\%$, $\varepsilon_{c,AlN} = -0.195\%$, implying that the in-plane strains of GaN and AlN are tensile, and the out-of-plane are compressive. All the calculations demonstrate that GaN epilayer of sample B with 460-nm-$Al_xGa_{1-x}N$-interlayer has the lowest in-plane tensile strain, which is in good agreement with the results of Raman measurements.

From the above discussion, we noticed that all the results consistently show that the optimum thickness of the $Al_xGa_{1-x}N$ interlayer to grow crack-free thick GaN film is 460 nm, which is much thin-

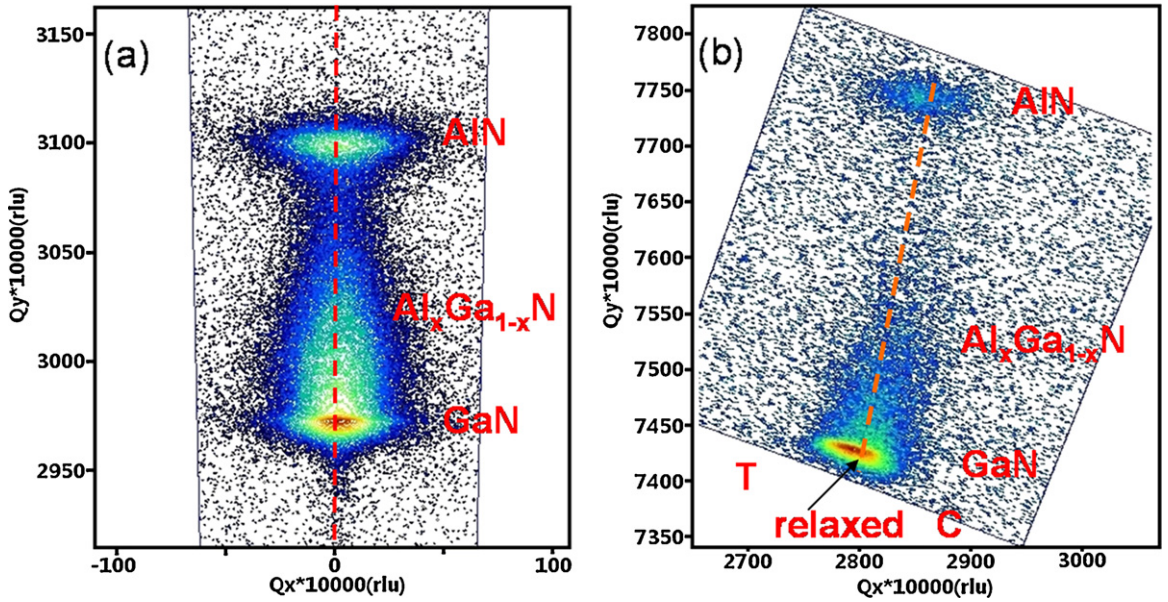

Fig. 6. (a) (0 0 0 2) and (b) ($10\bar{1}5$) RSMs of sample B with 460 nm-thick composition-graded $Al_xGa_{1-x}N$ interlayer.

ner compared with those reported in previous works [13–15]. These works also demonstrate that thicker $Al_xGa_{1-x}N$ interlayer can build up more compressive stress, thus promote the growth of thicker crack-free GaN films. However, in our work, the composition of $Al_xGa_{1-x}N$ interlayer changes nonlinearly, that is Ga-rich $Al_xGa_{1-x}N$ interlayer is thicker than the Al-rich $Al_xGa_{1-x}N$ interlayer. From this viewpoint, our work is more like the extremity of step-graded $Al_xGa_{1-x}N$ technique, in which an optimum thickness exists and varies with the different design [11]. In our case, we consider there are at least two effects working. One is the so called "V-trenches" effect, and the other one is the thickness effect as described above. For the former, the V-trenches, always formed during the growth of high Al content AlGaN and filled up by the subsequently grown $Al_xGa_{1-x}N$ or GaN, are believed to be able to alleviate the compressive strain [5,15]. When the $Al_xGa_{1-x}N$ interlayer is thin (sample A), the "V-trenches" effect dominates and $Al_xGa_{1-x}N$ interlayer fails to compensate the tensile stress effectively, resulting in the high crack density and tensile stress of GaN film. When the $Al_xGa_{1-x}N$ interlayer gets thicker (sample B), the V-trenches are all filled up, the thickness effect dominates, the compressive stress can be effectively accumulated by maintaining the 2-D growth mode, thus leading to the crack-free GaN films. On the other hand, graded AlGaN grown on AlN underlayer will be gradually relaxed by inclination of threading dislocation, and the extent of relaxation highly depends on the projection length of inclined dislocation line onto the growth plane, which is proportional to the inclination angle and the thickness of AlGaN layer film [23–26]. AlGaN layer with a larger thickness or with a larger inclination angle of dislocation will relax more significantly, and may not exert adequate compressive stress on GaN overlayer to compensate the tensile stress induced during cooling process. Therefore, it is expected that a thicker AlGaN interlayer may result in cracking of GaN films. The reason why the tensile stress in GaN film first ascends then descends with further increasing $Al_xGa_{1-x}N$ thickness (>460 nm) as samples C and D shows can be attributed to the complex interplay of thickness and dislocation inclination angle in AlGaN of different thickness, and more detailed study on microstructural evolution of graded AlGaN layer will be explored to understand this issue and the results will be reported later.

4. Conclusions

The surface morphology, crystalline quality and strain states of GaN films with continuously composition-graded $Al_xGa_{1-x}N$ interlayers on AlN/Si (1 1 1) templates have been investigated. It was found that the properties of GaN films are highly dependent on the thickness of $Al_xGa_{1-x}N$ interlayer and a small window exists to grow high quality crack-free GaN films. When the continuously composition-graded $Al_xGa_{1-x}N$ interlayer is around 460 nm thick, crack-free GaN films up to 1.2 μm with significantly reduced (0 0 0 2) FWHM and tensile stress was achieved.

Acknowledgements

This work was supported by the Doctoral Program Foundation of Institutions of Higher Education of China (Grant No. 200804871144), the Program for New Century Excellent Talents in University (NCET-08-0214), the Hubei Province Science Fund for Distinguished Young Scholars (Grant No. 2008CDB334), the Key Programs of the Natural Science Foundation of Huazhong University of Science and Technology (Grant No. 20072008B), the National Natural Science Foundation of China (Grant No. 60976042), the Open Project of State Key Laboratory of Functional Materials for Informatics, and the National Natural Science Foundation of China (Grant No. 60906023), the Major Program of National Natural Science Foundation of China (Grant No. 10990100), and the National Basic Research Program of China (973 Program: 2010CB923204).

References

[1] A. Krost, A. Dadgar, Mater. Sci. Eng. B 93 (2002) 77–84.
[2] J. Bläsing, A. Reiher, A. Dadgar, A. Diez, A. Krost, Appl. Phys. Lett. 81 (2002) 2722–2724.
[3] L.S. Chuah, Z. Hassan, H.A. Hassan, N.M. Ahmed, J. Alloys Compd. 481 (2009) L15–L19.
[4] K.P. Beh, F.K. Yam, C.W. Chin, S.S. Tneh, Z. Hassan, J. Alloys Compd. 506 (2010) 343–346.
[5] W. Liu, J.J. Zhu, D.S. Jiang, H. Yang, J.F. Wang, Appl. Phys. Lett. 90 (2007) 011914.
[6] D.K. Kim, J. Crystal Growth 312 (2010) 478–481.
[7] Y.X. Yu, J.J. Zhu, D.G. Zhao, Z.S. Liu, D.S. Jiang, S.M. Zhang, Y.T. Wang, H. Wang, G.F. Chen, H. Yang, Chin. Phys. B 18 (2009) 4413–4417.
[8] E. Feltin, B. Beaumont, M. Laügt, P. de Mierry, P. Vennéguès, H. Lahrèche, M. Leroux, P. Gilbart, Appl. Phys. Lett. 79 (2001) 3230–3232.
[9] S.H. Jang, C.R. Lee, J. Crystal Growth 253 (2003) 64–70.
[10] M.H. Kim, Y.G. Do, H.C. Kang, D.Y. Noh, S.J. Park, Appl. Phys. Lett. 79 (2001) 2713–2715.
[11] K. Cheng, M. Leys, S. Degroote, B. Van Daele, S. Boeykens, J. Derluyn, M. Germain, G. Van Tendeloo, J. Engelen, G. Borghs, J. Electron. Mater. 35 (2006) 592–598.
[12] C.C. Huang, S.J. Chang, R.W. Chuang, J.C. Lin, Y.C. Cheng, W.J. Lin, Appl. Surf. Sci. 256 (2010) 6367–6370.
[13] H. Marchand, L. Zhao, N. Zhang, B. Moran, R. Coffie, U.K. Mishra, J.S. Speck, S.P. Denbaars, J. Appl. Phys. 89 (2001) 7846–7851.
[14] A. Able, W. Wegscheider, K. Engl, J. Zweck, J. Crystal Growth 276 (2005) 415–418.
[15] S. Raghavan, J. Redwing, J. Appl. Phys. 98 (2005) 023515.
[16] M. Haeberlen, D. Zhu, C. McAleese, M.J. Kappers, C.J. Humphreys, J. Phys.: Conf. Ser. 209 (2010) 012017.
[17] K.L. Lin, E.Y. Chang, Y.L. Hsiao, W.C. Huang, T.T. Luong, Y.Y. Wong, T.K. Li, D. Tweet, C.H. Chiang, J. Vac. Sci. Technol. B 28 (2010) 473–477.
[18] M. Irie, N. Koide, Y. Honda, M. Yamaguchi, N. Sawaki, J. Crystal Growth 311 (2009) 2891–2894.
[19] K.W. Kim, D.S. Kim, J.H. Lee, J.H. Lee, C.K. Hahn, Electrochem. Solid-State Lett. 13 (2010) H66–H69.
[20] B. Kim, S. Jang, J. Jhin, S. Lee, J.H. Baek, Y. Yu, J. Lee, D. Byun, Jpn. J. Appl. Phys. 49 (2010) 021003.
[21] S. Tripathy, S.J. Chua, P. Chen, Z.L. Miao, J. Appl. Phys. 92 (2002) 3053–3510.
[22] M.A. Moram, M.E. Vickers, Rep. Prog. Phys. 72 (2009) 036502.
[23] P. Cantu, F. Wu, P. Waltereit, S. Keller, A.E. Romanov, U.K. Mishra, S.P. DenBaars, J.S. Speck, Appl. Phys. Lett. 83 (2003) 674.
[24] D.M. Follstaedt, S.R. Lee, P.P. Provencio, A.A. Allerman, J.A. Floro, M.H. Crawford, Appl. Phys. Lett. 87 (2005) 121112.
[25] P. Cantu, F. Wu, P. Waltereit, S. Keller, A.E. Romanov, S.P. DenBaars, J.S. Speck, J. Appl. Phys. 97 (2005) 103534.
[26] D.M. Follstaedt, S.R. Lee, A.A. Allerman, J.A. Floro, J. Appl. Phys. 105 (2009) 083507.